LETTER

Skin shedding and tissue regeneration in African spiny mice (*Acomys*)

Ashley W. Seifert[1,2,3], Stephen G. Kiama[2], Megan G. Seifert[1,3], Jacob R. Goheen[3,4], Todd M. Palmer[1,3] & Malcolm Maden[1]

Evolutionary modification has produced a spectrum of animal defence traits to escape predation, including the ability to autotomize body parts to elude capture[1,2]. After autotomy, the missing part is either replaced through regeneration (for example, in urodeles, lizards, arthropods and crustaceans) or permanently lost (such as in mammals). Although most autotomy involves the loss of appendages (legs, chelipeds, antennae or tails, for example), skin autotomy can occur in certain taxa of scincid and gekkonid lizards[3]. Here we report the first demonstration of skin autotomy in Mammalia (African spiny mice, *Acomys*). Mechanical testing showed a propensity for skin to tear under very low tension and the absence of a fracture plane. After skin loss, rapid wound contraction was followed by hair follicle regeneration in dorsal skin wounds. Notably, we found that regenerative capacity in *Acomys* was extended to ear holes, where the mice exhibited complete regeneration of hair follicles, sebaceous glands, dermis and cartilage. Salamanders capable of limb regeneration form a blastema (a mass of lineage-restricted progenitor cells[4]) after limb loss, and our findings suggest that ear tissue regeneration in *Acomys* may proceed through the assembly of a similar structure. This study underscores the importance of investigating regenerative phenomena outside of conventional model organisms, and suggests that mammals may retain a higher capacity for regeneration than was previously believed. As re-emergent interest in regenerative medicine seeks to isolate molecular pathways controlling tissue regeneration in mammals, *Acomys* may prove useful in identifying mechanisms to promote regeneration in lieu of fibrosis and scarring.

Among mammals, autotomy seems to have evolved several times, but is taxonomically sparse. Documented autotomy is typically restricted to the tail and occurs through loss of the tail sheath (false autotomy) or through breakage across the vertebra (true autotomy)[2,5]. In addition to tail autotomy, casual reference has been made to mammalian species with weak or fragile skin, although whether these animals are capable of skin autotomy remains unknown. Thus, we first sought to investigate anecdotal evidence that two species of African spiny mouse (*Acomys kempi* and *Acomys percivali*) readily shed portions of their skin as a predator escape behaviour.

To test the hypothesis that *A. kempi* and *A. percivali* are capable of skin autotomy, we live-trapped individuals on rocky outcroppings (kopjes) in central Kenya. In addition to guard hairs, species in the genus *Acomys* are notable for the presence of spine-like hairs on the dorsum (Fig. 1a, b). Handling both species in the field confirmed that vigorous movement often led to tearing of the skin. Tearing resulted in large open wounds or skin loss ranging from small pieces to areas approximating 60% of the total dorsal surface area (Fig. 1c). In addition to integumentary loss, both species exhibited autotomy of the tail sheath as previously reported for other *Acomys* species, and individuals were often captured with missing tails[2]. Among captive individuals, we observed severe skin wounds to heal quickly, and rapid regrowth of spiny hairs totally obscured the wounded area (Fig. 1d, e). Field-captured individuals showed similar healing and, in some cases,

patterned hair follicles in anagen (growth phase) that seemed to have regenerated in wounded areas (Fig. 1f).

To evaluate how *Acomys* skin tears so easily, we asked whether the mechanical properties of *Acomys* skin might underlie its observed weakness. On the basis of experiments investigating skin autotomy in geckos[3], weak skin (that is, skin possessing uniform structural properties that fails or breaks under relatively low induced loading) can be differentiated from fragile skin (that is, skin possessing specific morphological characterizations such as a fracture plane that allows the outer layers to be released). To assess skin weakness, we compared mechanical properties of *Acomys* and *Mus* skin. During mechanical loading, *Mus* skin displayed elastic properties before breaking, whereas *Acomys* skin was brittle and began tearing shortly after load was applied (Fig. 2a). We derived stress–strain curves from dorsal skin to determine the mean tensile strength (σ_m) and found that *Mus* skin was 20 times stronger than *Acomys* skin (2.3 ± 0.19 MPa and
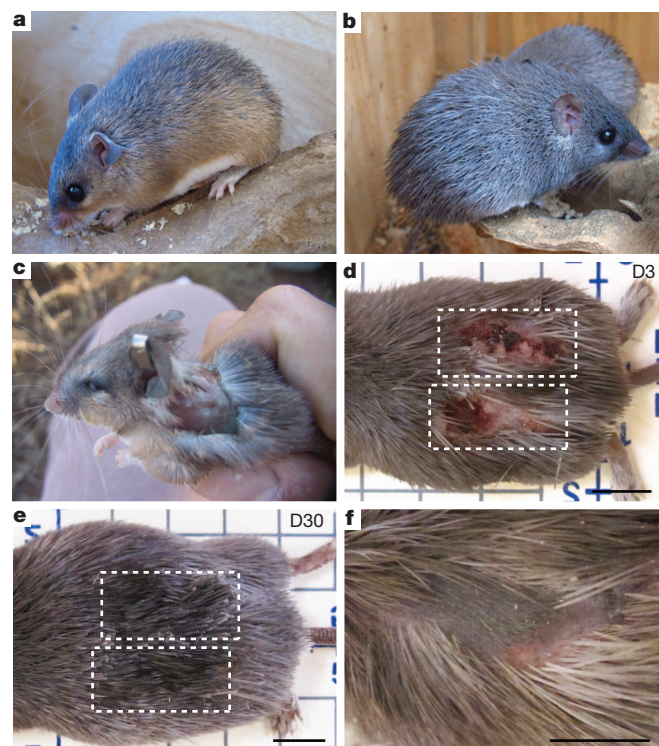

Figure 1 | *A. kempi* and *A. percivali* exhibit skin autotomy and subsequent rapid healing. a, b, *A. kempi* (**a**) and *A. percivali* (**b**) possess stiff, spine-like hairs on the dorsum. **c,** *A. kempi* after loss of dorsal skin. **d, e,** Scab formation after full-thickness skin injury visible at D3 (**d**). The same wounds in **d** are no longer visible at D30 (**e**), and new spiny hairs cover the damaged area at D30 (**e**). **f,** Healing wound in field-caught specimen showing new hair follicles within the wound bed. Scale bars, 1 cm.

[1]Department of Biology, University of Florida, 223 Bartram Hall, PO Box 118525 Gainesville, Florida 32610, USA. [2]Department of Veterinary Anatomy and Physiology, University of Nairobi, PO Box 30197, 00010 Nairobi, Kenya. [3]Mpala Research Centre, PO Box 555 Nanyuki 10400, Kenya. [4]Department of Zoology and Physiology, and Department of Botany, University of Wyoming, 1000 East University Avenue, Laramie, Wyoming 82071, USA.

0.11 ± 0.03 MPa (mean ± s.e.m.)) (Fig. 2a, b). Lastly, by calculating mean toughness (W), we found that nearly 77 times more energy was required to break *Mus* skin relative to *Acomys* skin (Fig. 2b). These results demonstrate that *Acomys* possess skin that tears (or breaks) easily in response to low applied tension and provide a mechanical basis for the weakness of their skin.

To evaluate whether structural properties of *Acomys* skin contributed to its mechanical weakness, we examined cellular features of *A. percivali* skin and found that it was anatomically comparable to that of *Mus* and other rodents, albeit with much larger hair follicles (Fig. 2c, d). We found no evidence of a fracture plane, which is the mechanism of skin autonomy in geckos and skinks[3]. Examining elastin fibres, which enhance skin elasticity, we found all three species possessed a similar distribution and abundance of elastin in the dermis and beneath the panniculus carnosus (Supplementary Fig. 1a–f). We tested whether larger hair follicles in *Acomys* skin reduced the total dermal area occupied by connective tissue by examining the proportion of adnexa (that is, follicles and associated glands) within the dermis and found it was greater in *A. percivali* (55.61 ± 4.28%) compared with *M. musculus* (43.65 ± 4.62%) ($t = 1.9$, $P = 0.043$) (Fig. 2e, f). These findings suggest that although the basic tissue structure of *Acomys* skin is similar to *Mus*, the space occupied by adnexa in the dermis reduces the absolute connective tissue content, potentially contributing to the decreased elasticity and lower tensile strength when the skin is placed under tension[6]. The lack of a fracture plane underscores this finding and supports an inherent structural difference underlying the observed weakness of *Acomys* skin.

Given its inherent structural weakness and propensity to tear, we assessed the ability of *Acomys* to heal skin wounds using small (4 mm) and large (1.5 cm), full-thickness excisional wounds. Scab formation and haemostasis was rapid in wounds of both sizes and the wound area in large wounds was reduced by 64 ± 3.1% 24 h after injury (Supplementary Fig. 2a). During scar-free healing in terrestrial salamanders[7] and mammalian fetuses[8], the wound bed is re-epithelialized within several days, whereas a 4-mm wound in adult rat skin takes between

5 and 7 days to re-epithelialize[9]. In *Acomys*, we found that five out of six 4-mm wounds had completely re-epithelialized by day 3 after injury (D3), whereas *Mus* wounds failed to re-epithelialize this quickly (Fig. 2g, h). After re-epithelialization, loose-skinned mammals (such as rodents and rabbits, for example) rely primarily on contraction to heal their wounds[10]. Similarly, we observed high contraction rates, which accounted for 95% of wound closure after 17 days (Supplementary Fig. 2a–c). In contrast to scarring, in which collagen fibres organize into a dense network parallel to the epidermis, during scar-free healing collagen fibres assume a pattern similar to unwounded dermis[10]. Examining the extracellular matrix (ECM) at D10, we observed scarring in *Mus*, whereas in *Acomys*, collagen fibres were less densely packed and contained a more porous structure (Fig. 2i, j). Using picrosirius red we found collagen type I predominated the wound bed at D10 in *Mus*, whereas collagen type III was in greater abundance in *Acomys* (Fig. 2k, l). This difference was even more pronounced in 1.5-cm wounds (Supplementary Fig. 3a–b'). Together, these data show that rapid re-epithelialization and wound edge contraction greatly reduce the size of open skin tears in *Acomys*. Our findings, that wound ECM is deposited slowly, has a porous configuration and is dominated by type III collagen, suggest that this composition favours regeneration over fibrosis during skin repair in *Acomys*.

To test the regenerative capacity of the wound environment we sampled large healing wounds for evidence of hair follicle neogenesis and dermal regeneration. In association with the more porous ECM, we observed folliculargenesis of normal pelage hairs and large spiny hairs in the wound bed between D21 and D28 and we could distinguish old, large follicles near the wound margins from newly regenerated follicles within the wound bed (Fig. 3a–d and Supplementary Fig. 3c–e). New follicles seemed to regenerate throughout the uncontracted portion of the wound bed not just in the central region (Fig. 3c and Supplementary Fig. 3e), and we observed regenerating hair follicles in various stages of development (Fig. 3a–m and Supplementary Fig. 4a–c). A localized and highly proliferative population of epidermal cells drives hair follicle development
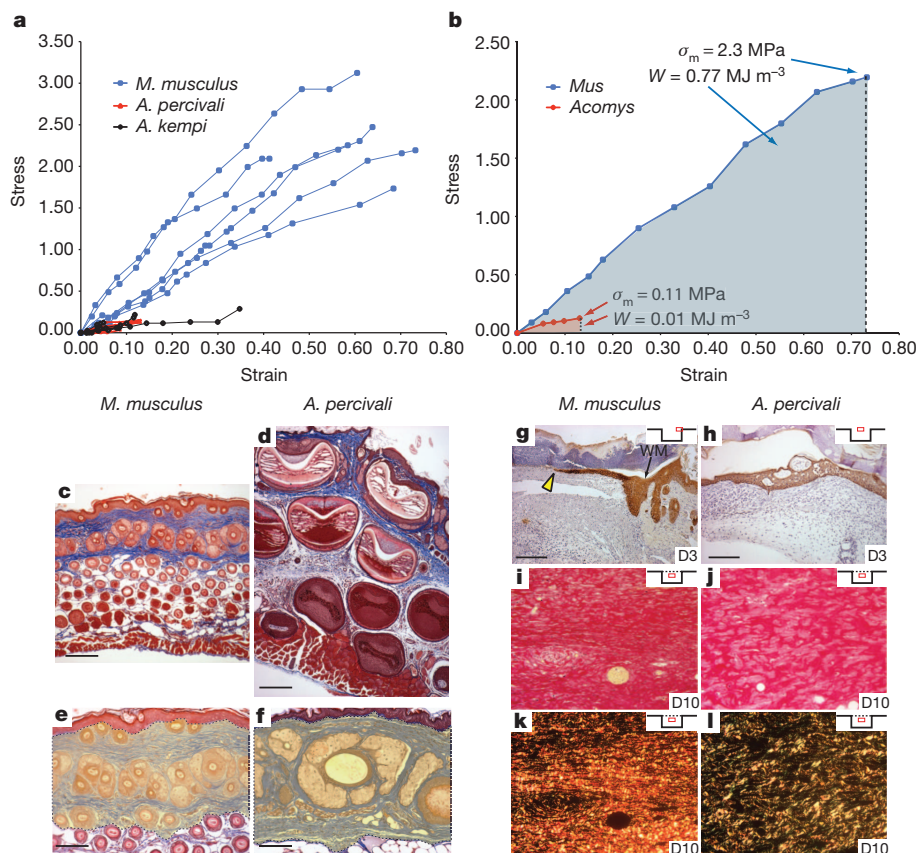

Figure 2 | *Acomys* skin is weak, tears easily, and during repair develops a porous ECM rich in collagen type III. a, b, Stress–strain curves for *M. musculus* ($n = 6$), *A. kempi* ($n = 5$) and *A. percivali* ($n = 5$), depicted up to the failure strain (**a**) and for one individual (**b**) approximating the real mean tensile strength (σ_m) and mean toughness (W) (represented as shaded area). **c, d,** Masson's trichrome staining of unwounded back skin from *M. musculus* (**c**) and *A. percivali* (**d**). **e, f,** The proportion of adnexa (hair follicles and associated glands) in the dermis (yellow shading) of *M. musculus* (**e**) and *A. percivali* (**f**). **g,** Cytokeratin-stained keratinocytes (yellow arrowhead) just beginning to migrate in small wounds at D3 in *M. musculus*. **h,** Completely re-epithelialized wounds in *Acomys* at D3. WM, wound margin. Insets show relative wound position of the pictured tissue. **i–l,** Picrosirius red staining of small wounds in *M. musculus* (**i, k**) and *A. percivali* (**j, l**). Bifringence of picrosirius stain (**k, l**) differentiates thick collagen type I fibres (red/orange) from thin collagen type III fibres (green). Collagen fibres in *M. musculus* are predominantly type I, densely packed and run parallel to the epidermis (**k**). Collagen fibres in *A. percivali* are more porous with a greater proportion of collagen type III (**l**). Scale bars, 100 μm.

and we observed a similar phenomenon during follicle regeneration (Fig. 3e and Supplementary Fig. 4a–c). To investigate whether embryonic signalling networks used during hair follicle development were used during hair follicle regeneration, we examined keratin 17 (*KRT17*), which is diffusely expressed within the epidermis during skin development and becomes progressively restricted to developing hair follicles[11]. After re-epithelialization, KRT17 was highly enriched throughout the neoepidermis overlying the wound bed at D14, and as new hair follicles formed in the wound bed, KRT17 became restricted to follicular epithelium (Fig. 3f and Supplementary Fig. 5). During wound repair in *Mus*, we found KRT17 was also highly upregulated in the re-epithelialized epidermis at D14 (Supplementary Fig. 5), and although KRT17 localized to some basal keratinocytes in *Mus* epidermis at D21, these sites failed to aggregate into placodes or new hair follicles such that KRT17 was completely absent from the new epidermis by D26 (Fig. 3f). The disappearance of KRT17 from basal keratinocytes in *Mus*, together with our observation of continued localization in new placodes and hair follicles in *Acomys*, suggests the underlying dermal signals required to induce placode formation in *Mus* are lacking.

Although the precise signal for placode formation remains obscure, there is an absolute requirement for Wnt-signalling during normal follicle formation[12]. Nuclear localization of LEF1 protein has been used as a readout of this inductive signalling[13]. We detected nuclear accumulation of LEF1 in regenerating epidermal placodes, condensing dermal fibroblasts beneath the hair germ, and in dermal papilla and matrix cells (Fig. 3g, h and Supplementary Fig. 6a). We also detected nuclear LEF1 staining at low levels in some non-placode basal keratinocytes, whereas we did not detect nuclear LEF1 in the epidermis during wound healing in *Mus*, suggesting epidermal Wnt-activation in *Acomys* may partially underlie our observation of hair follicle regeneration (Supplementary Fig. 6b, c).

Regulation of canonical Bmp-signalling also has a role during hair follicle induction and differentiation of follicular progenitor populations into the mature hair follicle (reviewed in ref. 14). Phosphorylation of SMAD proteins 1, 5 and 8 (pSMAD1, 5 and 8) is a robust readout of canonical Bmp signalling. We detected pSMAD1/5/8 (the antibody detects the phosphorylated forms of all of these proteins but does not exclusively differentiate any particular one) at low levels during follicle induction and later at higher levels in dermal papilla and matrix cells undergoing differentiation in the hair bulb (Fig. 3i, j). Furthermore, we detected SOX2-positive dermal papilla in some regenerating hair follicles, which is consistent with its role in specifying various hair types during mouse hair follicle development[15] (Fig. 3k). Taken together, these results demonstrate that regenerating hair follicles in *Acomys* progress through defined stages of hair follicle development, exhibit high rates of proliferation, and reuse molecular pathways used during embryonic hair follicle development to regenerate new hair follicles.

Adult mammal skin is normally unable to regenerate epidermally-derived structures in response to wounding (for example, glands and hair follicles). An exception to this is the observation of spontaneous folliculargenesis in large excisional wounds in rabbits, and more recently in laboratory mice (C57BL6/SJ, SJL or mixed strain)[16–18]. Rabbits are also one of the few mammalian species that can regenerate large ear punch wounds[19]. We proposed that the regenerative capacity observed in *Acomys* might extend to their ear tissue as well. To test this we made 4-mm punches through the ears of both *Acomys* species and, to our surprise, found that they were able to close these large punches (Fig. 4a–c and Supplementary Fig. 7a–c). Uninjured ear tissue contains skin (epidermis and dermis), associated hair follicles, adipose cells, muscle and cartilage; we found that *Acomys* were capable of completely regenerating all of these tissues with high fidelity except muscle (Fig. 4b, c). Twelve days after injury we observed an accumulation of cells around the circumference of the wound beneath the epidermis, and, although regeneration of new tissue was centripetal, cells accumulated to a greater degree on the proximal side of the punch. Hair follicle and cartilage regeneration proceeded in a proximal to
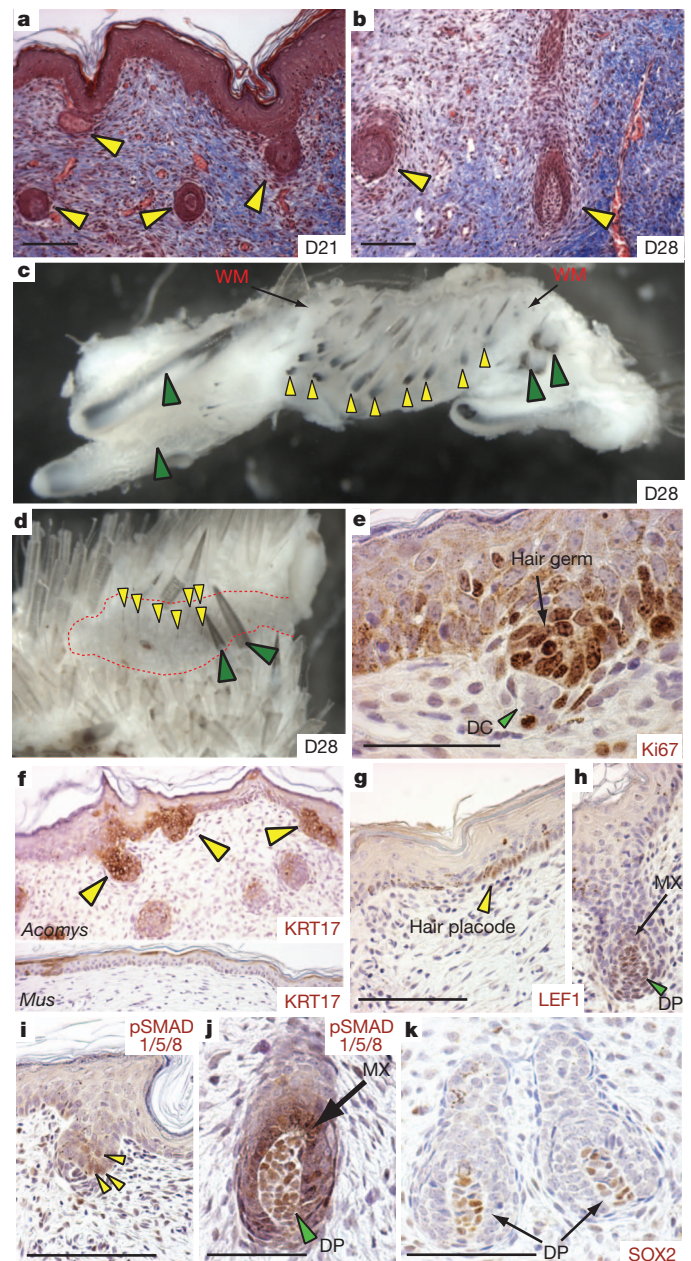

Figure 3 | *Acomys* exhibit *de novo* hair follicle regeneration in wounded skin. a–d, Hair follicles regenerating in *A. percivali* (yellow arrowheads) between D21 and D28 in large skin wounds. New hair follicles (yellow arrowheads) are present throughout the wound bed (red dotted area) at D28 (**c, d**). Green arrowheads indicate old follicles. **e–k**, Regenerating hair follicles express proteins associated with development and differentiation. Ki67 labels proliferating hair germ (**e**). KRT17 (yellow arrowheads) is present in *Acomys* but absent in *Mus* at D26 (**f**). Nuclear-localized LEF1 is present in follicle placodes (**g**) and later in dermal papilla cells (DP) and surrounding matrix cells (MX) (**h**). Phosphorylated SMAD1, 5 and 8 (as a readout of Bmp-signalling) is present in epidermal hair germ cells (**i**) and later in dermal papilla and matrix cells of regenerating follicles (**j**). SOX2 is present in dermal papilla cells (**k**). Scale bars, 100 μm (**a–d**, **f–k**) and 50 μm (**e**).

distal wave (Fig. 4d, e) and similar to the skin, follicular epidermis in the ear activated Wnt-signalling (Supplementary Fig. 6d, e). In contrast to *Acomys*, we found *Mus* were incapable of regenerating 4-mm ear punches and instead formed scar tissue (Supplementary Fig. 8a, b). Notably, despite scar formation, *Mus* ear repair resulted in the *de novo* formation of cartilage condensations distal to the cut cartilage suggesting *Mus* might initiate, but not maintain, a regenerative response after ear wounding (Supplementary Fig. 8b).

It remains unclear whether mammalian regeneration proceeds through formation of a blastema, or is instead an exaggerated version of hyperplastic growth[20–22]. Blastema formation is considered a hallmark of epimorphic regeneration. One characteristic of a regeneration blastema is that it contains proliferating cells and maintains proliferation during regeneration[23]. We observed widespread proliferation throughout the ear regenerate in *Acomys* and surprisingly, throughout healing ear tissue in *Mus* (Fig. 4f, g). However, we noted a lack of proliferation in the distal epidermis of *Acomys*, whereas we detected proliferation throughout *Mus* epidermis extending to the distal tip (Fig. 4f, g). Although proliferation was maintained in *Acomys* ears, we observed almost no proliferating cells in later-staged *Mus* ears (Fig. 4h, i).

A second characteristic of a blastema is the formation of a specialized epidermal signalling centre (the wound epidermis), which is required for proliferating blastemal cells to remain in the cell cycle[24] and is characterized by a loss of epidermal stratification, loss of basal keratinocyte polarity, and lack of a mature basal lamina[25]. After re-epithelialization in *Acomys*, we noted a thickening of the distal epidermis, disorganization of basal keratinocytes and absence of a mature basement membrane (Fig. 4j). Comparatively, the epidermis near the amputation plane exhibited normal stratification and possessed a prominent basement membrane (Fig. 4k). By contrast,

Mus seemed to form a wound epidermis only transiently after re-epithelialization, with a proportionately smaller distal area exhibiting these characteristics for a short time (data not shown). By D12 in *Mus*, collagen type IV staining revealed a mature basement membrane beneath the entire epidermis of the healing ear (Fig. 4l). In addition, the epidermis exhibited normal stratification and proper apical-basal polarity of the basal keratinocytes (Fig. 4g, l).

In addition to sustained proliferation and formation of the wound epidermis, ECM molecules have a key role in supporting proliferation and directing subsequent differentiation during regeneration[26]. By contrast, molecules such as laminin and collagen type I, which favour differentiation, are downregulated in the blastema during amphibian limb regeneration and are expressed as differentiation of the musculoskeletal system proceeds[26,27]. Histological examination of *Acomys* ears at D12 revealed high levels of fibronectin, some tenascin-C (TN-C) surrounding densely packed cells, but very low levels of collagen type I (Supplementary Fig. 9a–c). Collagen type III was also more abundant than collagen type I during regeneration (Supplementary Fig. 9d–d'). TN-C became restricted from areas where new cartilage began differentiating and within these differentiating cells we found activation of the Bmp-signalling pathway in cells giving rise to new auricular cartilage (Fig. 4o and Supplementary Fig. 10). During hyperplastic growth in *Mus* ears, the ECM initially displayed
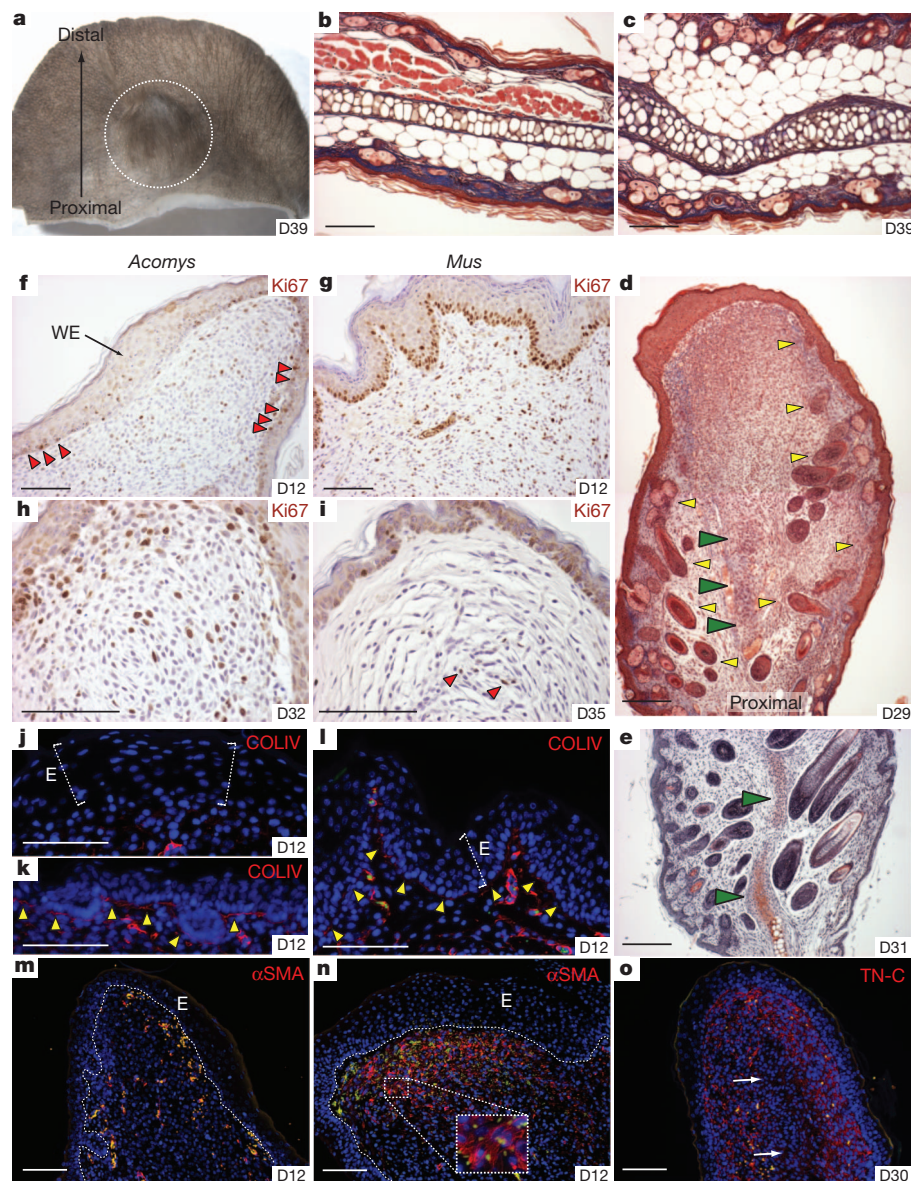

Figure 4 | *Acomys* regenerate hair follicles, sebaceous glands, dermis, adipose tissue and cartilage in 4-mm ear punches. a, A regenerated 4-mm ear punch in *A. percivali*. **b**, Unwounded tissue in *Acomys* ear pinna. **c**, Regenerated dermis, hair follicles, cartilage and adipose tissue within biopsy punched area. White circle denotes the original punch area. **d**, Regenerating hair follicles (yellow arrowheads) and cartilage (green arrowheads) differentiate proximal to distal. **e**, Safranin-O and fast green staining indicates chondrogenesis (green arrowheads). **f–i**, Proliferating cells (Ki67^{+}) in early (**f**, **g**) and late (**h**, **i**) *Acomys* and *Mus* ears. Proliferation is restricted proximal to the wound epidermis (WE) (red arrowheads) in *Acomys* (**f**) and is continuous in basal keratinocytes of *Mus* (**g**). Proliferation is maintained in *Acomys* at D32 (**h**) with very few proliferating cells persisting in *Mus* (**i**) (red arrowheads). **j–l**, Collagen-IV-stained mature basement membrane is absent beneath the wound epidermis (E) in *Acomys* (**j**), but is present near the amputation (**k**) and distally in *Mus* (**l**). Yellow arrowheads indicate basement membrane, and white lines indicate epidermal thickness. **m, n**, Almost no αSMA-positive fibroblasts are present in *Acomys* (**m**), whereas αSMA-positive myofibroblasts are present in healing *Mus* ear (**n**). Inset shows stress fibres in individual myofibroblasts. **o**, TN-C disappears where new cartilage differentiates (white arrows) in *Acomys*. Yellow/green cells (**j–o**) are autofluorescing blood cells in the green fluorescent protein (GFP) channel. Scale bars, 100 μm.

high levels of fibronectin and low levels of TN-C as did *Acomys* ears, but produced relatively higher levels of collagen type I (Supplementary Fig. 9e–g). Collagen production in *Mus* was not only faster and more abundant, but also exhibited a higher ratio of collagen type I to type III (Supplementary Fig. 9h, h'). Given the exuberant production of collagen type I in *Mus*, we asked whether resident fibroblasts were differentiating into myofibroblasts, which contribute to scarring in lieu of regeneration (reviewed in ref. 28). Using α-smooth muscle actin (αSMA), we found myofibroblasts in high abundance throughout ear tissue in *Mus*, whereas they were almost completely absent in *Acomys* ears (Fig. 4m, n). These data corroborate the importance of the wound ECM to promote proliferation while antagonizing differentiation and support previous work showing precocious collagen type I formation antagonizes appendage regeneration[27].

Our data suggest that reparative ear regeneration in *Acomys* is a balance between premature reformation of the dermis (scarring) and maintenance of cell proliferation within a pro-regenerative environment. By contrast, *Mus* fails to form (or maintain) a wound epidermis, which is coincident with precocious formation of the basement membrane and stratification of the epidermis. This leads to a loss of cell proliferation, increased collagen type I deposition (in lieu of collagen type III), myofibroblast activation and ultimately, scar formation. Although our data suggest ear regeneration shares similar characteristics with blastema formation, understanding the molecular signals required to organize and maintain a wound epidermis and identifying the lineage of regenerating cells is crucial to address how regeneration occurs in these animals. Future work investigating how *Acomys* can control fibrosis will shed light on how regeneration and scarring can be balanced in the face of infection and inflammation in wild mammals, and provides an ideal model system in which to examine epimorphic regeneration in mammals.

METHODS SUMMARY

Animals. Specimens of *A. kempi* and *A. percivali* were live-captured in Laikipia, Kenya, at the Mpala Research Centre. Experimental animals were held in an open-air field laboratory under ambient conditions. For comparative experiments, Swiss Webster mice were obtained from a local supplier in Nairobi and in the United States from Charles River.

Wounding. All experiments conducted in Kenya were performed in accordance with approved animal practices. Experiments performed in the United States were approved by the Institutional Review Board on Animal Care at the University of Florida and in Kenya by the University of Nairobi. Spiny mice were halothane-anaesthetized and small (4 mm) and large (1.5 cm) full-thickness excisional wounds were made on the dorsum.

Strength measurements. Strength measures were made using a Hounsfield tensometer equipped with an automatic motor and stretched at a rate of 20 mm min^{-1}. Full-thickness skin strips (including the panniculus carnosus) measuring approximately 20×40 mm were used. Force (N) and displacement (mm) were measured on a *xy* plotter and these points were subsequently recorded as stress (σ = force per cross-sectional area) and strain (ε = change in length/initial length) and replotted in Excel. The work (W) required to achieve the breaking strength was calculated as the area under each stress–strain curve and expressed as the mean work for each genus.

Histology and immunohistochemistry. For histological analysis, samples were fixed in 10% neutral buffered formalin at 4 °C for 16–24 h, washed in PBS, dehydrated in ethanol and infiltrated with paraffin. Samples were cut at 5 µm. For immunohistochemistry, slides were incubated with primary antibodies (see Methods) and visualized using either 3,3'-diaminobenzidine (DAB) or Alexa-Flour 594. Negative controls were run using appropriate Ig isotypes at the same concentration as the primary antibody. For all immunohistochemistry comparisons, a minimum of $n = 4$ per species was used.

Full Methods and any associated references are available in the online version of the paper.

Received 27 November 2011; accepted 10 August 2012.

1. Maginnis, T. L. The costs of autotomy and regeneration in animals: a review and framework for future research. *Behav. Ecol.* **17**, 857–872 (2006).
2. Shargal, E., Rath-Wolfson, L., Kronfeld, N. & Dayan, T. Ecological and histological aspects of tail loss in spiny mice (Rodentia: Muridae, *Acomys*) with a review of its occurrence in rodents. *J. Zool.* **249**, 187–193 (1999).
3. Bauer, A. M., Russell, A. P. & Shadwick, R. E. Mechanical properties and morphological correlates of fragile skin in gekkonid lizards. *J. Exp. Biol.* **145**, 79–102 (1989).
4. Kragl, M. *et al.* Cells keep a memory of their tissue origin during axolotl limb regeneration. *Nature* **460**, 60–65 (2009).
5. Dubost, G. & Gasc, J.-P. The process of total tail autotomy in the South-American rodent, *Proechimys. J. Zool.* **212**, 563–572 (1987).
6. Vogel, H. G. Correlation between tensile-strength and collagen content in rat skin — effect of age and cortisol treatment. *Connect. Tissue Res.* **2**, 177–182 (1974).
7. Seifert, A. W., Monaghan, J. R., Voss, S. R. & Maden, M. Skin regeneration in adult axolotls: a blueprint for scar-free healing in vertebrates. *PLoS One* **7**, e32875 (2012).
8. Dang, C. M. *et al.* Scarless fetal wounds are associated with an increased matrix metalloproteinase-to-tissue-derived inhibitor of metalloproteinase ratio. *Plast. Reconstr. Surg.* **111**, 2273–2285 (2003).
9. Soo, C. *et al.* Differential expression of matrix metalloproteinases and their tissue-derived inhibitors in cutaneous wound repair. *Plast. Reconstr. Surg.* **105**, 638–647 (2000).
10. Yannas, I. V. *Tissue and Organ Regeneration in Adults* (Springer, 2001).
11. McGowan, K. M. & Coulombe, P. A. Onset of keratin 17 expression coincides with the definition of major epithelial lineages during skin development. *J. Cell Biol.* **143**, 469–486 (1998).
12. Andl, T., Reddy, S. T., Gaddapara, T. & Millar, S. E. WNT signals are required for the initiation of hair follicle development. *Dev. Cell* **2**, 643–653 (2002).
13. DasGupta, R. & Fuchs, E. Multiple roles for activated LEF/TCF transcription complexes during hair follicle development and differentiation. *Development* **126**, 4557–4568 (1999).
14. Botchkarev, V. A. & Sharov, A. A. BMP signaling in the control of skin development and hair follicle growth. *Differentiation* **72**, 512–526 (2004).
15. Driskell, R. R., Giangreco, A., Jensen, K. B., Mulder, K. W. & Watt, F. M. Sox2-positive dermal papilla cells specify hair follicle type in mammalian epidermis. *Development* **136**, 2815–2823 (2009).
16. Billingham, R. E. & Russell, P. S. Incomplete wound contracture and the phenomenon of hair neogenesis in rabbits' skin. *Nature* **177**, 791–792 (1956).
17. Breedis, C. Regeneration of hair follicles and sebaceous glands from the epithelium of scars in the rabbit. *Cancer Res.* **14**, 575–579 (1954).
18. Ito, M. *et al.* Wnt-dependent de novo hair follicle regeneration in adult mouse skin after wounding. *Nature* **447**, 316–320 (2007).
19. Vorontsova, M. A. & Liozner, L. D. *Asexual propagation and Regeneration* 377–379 (Pergamon, 1960).
20. Borgens, R. B. Mice regrow the tips of their foretoes. *Science* **217**, 747–750 (1982).
21. Muneoka, K., Allan, C. H., Yang, X., Lee, J. & Han, M. Mammalian regeneration and regenerative medicine. *Birth Defects Res. C Embryo Today* **84**, 265–280 (2008).
22. Clark, L. D., Clark, R. K. & Heber-Katz, E. A new murine model for mammalian wound repair and regeneration. *Clin. Immunol. Immunopathol.* **88**, 35–45 (1998).
23. Chalkley, D. T. A quantitative histological analysis of forelimb regeneration in *Triturus viridescens. J. Morphol.* **94**, 21–70 (1954).
24. Globus, M., Vethamany-Globus, S. & Lee, Y. C. Effect of apical epidermal cap on mitotic cycle and cartilage differentiation in regeneration blastemata in the newt, *Notophthalmus viridescens. Dev. Biol.* **75**, 358–372 (1980).
25. Neufeld, D. A. & Day, F. A. Perspective: a suggested role for basement membrane structures during newt limb regeneration. *Anat. Rec.* **246**, 155–161 (1996).
26. Calve, S., Odelberg, S. J. & Simon, H. G. A transitional extracellular matrix instructs cell behavior during muscle regeneration. *Dev. Biol.* **344**, 259–271 (2010).
27. Satoh, A., Makanae, A., Hirata, A. & Satou, Y. Blastema induction in aneurogenic state and Prrx-1 regulation by MMPs and FGFs in *Ambystoma mexicanum* limb regeneration. *Dev. Biol* **355**, 263–274 (2011).
28. Hinz, B. Formation and function of the myofibroblast during tissue repair. *J. Invest. Dermatol.* **127**, 526–537 (2007).

Author Contributions A.W.S., J.R.G., T.M.P. and M.M. formulated the research. A.W.S, M.G.S, M.M. and S.G.K., performed the research and analysed the data. A.W.S. wrote the manuscript and all authors discussed the results, commented on and edited the manuscript.

METHODS

Animals. Male and female *A. kempi* and *A. percivali* were live-captured using Sherman traps in Laikipia, Kenya, at the Mpala Research Centre, between 2009 and 2011. Fifty traps were set in the late afternoon at various kopjes (rock outcroppings), and traps were checked the next morning for animals. Captured animals were transported to an open-air field laboratory and held under ambient conditions in species-specific groups with access to water *ad libitum*. Animals were fed twice daily on peanut butter and oats. Some animals were transported to the University of Nairobi, where they were maintained under similar conditions. For comparative experiments, Swiss Webster mice were obtained from a local supplier in Nairobi and in the United States from Charles River.

Wounding. All experiments conducted in Kenya were performed in accordance with approved animal practices. Experiments performed in the United States were approved by the Institutional Review Board on Animal Care at the University of Florida and in Kenya by the University of Nairobi. Both male and female mice were used, but pregnant females were excluded. Three types of wounds were used for this study: natural wounds, small circular wounds (4 mm diameter), and large circular wounds (1.5 cm diameter). Spiny mice were halothane-anaesthetized and shaved at least 1 day before wounding. Natural wounds were not made by the investigators and occurred either in the field or in captivity. Full-thickness excisional wounds were made by pinching the skin with forceps and cutting beneath to form a 4-mm circle (small) or cutting with iridectomy scissors a 1.5-cm diameter circle (large). For small wounds, four wounds were made on the dorsum posterior to the forelimbs and anterior to the hindlimbs. Wounds were allowed to heal and were not treated during healing. Calipers were used to measure wound width (mm) and wounds were recorded using a Canon S900 ($\times 1$–$\times 4$ Macro zoom).

Strength measurements. After culling, the entire dorsal skin including the panniculus carnosus was removed and placed face down in PBS. Two strips of dorsal skin measuring 20×40 mm were excised from this preparation maintaining the anteroposterior orientation, and the second strip was returned to PBS while the first strip was measured. Strips for mechanical testing were placed in metal screw clamps with rubber pieces covering the clamped ends. Clamps were placed in a Hounsfield tensometer equipped with an automatic motor and stretched at a rate of 20 mm min^{-1}. Tissue measurements for width (mm) and length (mm) between clamps were measured before stretching, and PBS was applied before loading to keep the samples moist. Force (N) and displacement (mm) were measured on a xy plotter, and these points were subsequently recorded as stress (σ = force per cross-sectional area) and strain (ε = change in length/initial length) and replotted in Excel.

Load was applied to skin strips parallel to the long body axis and the tensile strength (σ_m) and failure strain (ε_f) were recorded (*M. musculus* ($n = 6$), *A. kempi* ($n = 5$) and *A. percivali* ($n = 5$)). The work (W) required to achieve the breaking strength was calculated as the area under each stress–strain curve and expressed as the mean work for each genus.

Histology and immunochemistry. For histological analysis, samples were fixed in 10% neutral buffered formalin at $4\,^{\circ}\text{C}$ for 16–24 h, washed in PBS, dehydrated in ethanol and infiltrated with paraffin. Samples were cut at 5 μm. For immunohistochemistry, slides were incubated with primary antibodies (see Methods) and visualized using either 3,3'-diaminobenzidine (DAB) or Alexa-Flour 594. Negative controls were run using appropriate Ig isotypes at the same concentration as the primary antibody. For all immunohistochemistry comparisons, a minimum of $n = 4$ per species was used.

Primary antibodies and antigen retrieval used were: tenascin-C (1:50; Abcam; ab3970) with pronase at 1 μg ml^{-1} for 10 min at room temperature; fibronectin (1:500; Abcam; ab23750) with heat-induced epitope retrieval (HIER) in citrate buffer (pH 6.0); pan-cytokeratin (1:1,000; DAKO; Z0622) with proteinase K (DAKO) for 2 min at room temperature; cytokeratin 17 (1:400; Abcam; ab53707) with proteinase K for 2 min; Ki67 (1:2,000; Abcam; ab15580) with HIER in Tris-EDTA (pH 9.0); LEF1 (1:4,000; gift from O. Huber) with HIER in citrate buffer (pH 6.0) followed by treatment with 0.1% trypsin for 10 min room temperature; β-catenin (1:1,000; Sigma; HPA 029159) with HIER in citrate buffer (pH 6.0); pSMAD1/5/8 (1:200; Cell Signaling; 9511) with HIER in Tris-EDTA (pH 9.0); SOX2 (1:150; Abcam; ab97959) with HIER in citrate buffer (pH 6.0); collagen type IV (1:500; Rockland; 600-401-106-0.1) with proteinase K for 2 min; αSMA (1:200; Abcam; ab32575) with HIER in citrate buffer (pH 6.0); collagen type I (1:500; Abcam; ab34710) with HIER in citrate buffer (pH 6.0) followed by proteinase K for 2 min. For detection of rabbit antibodies, Vector Elite anti-rabbit kits were used, and for mouse monoclonal antibodies (TN-C) Vector M.O.M. kits were used. Antibodies were visualized with either diaminobenzidine (DAB) (Vector) or a streptavidin-conjugated Alexa-Flour 594 antibody after incubation with biotinylated anti-secondary.

Estimation of the proportion of the adnexa in the dermis. The volume density of the adnexa in the dermis $V_{V(\text{adnexa, dermis})}$ is the ratio of the total volume of follicles and sebaceous glands to the total volume of the dermis. This ratio can be estimated by point counting on plane sections[29–31]. For this purpose, one histological section was randomly sampled from each animal ($n = 6$ per species). The corresponding micrographs were projected on a screen, and a transparent test grid bearing a square lattice of points overlaid with random positions on each projected image:

$$V_{V(\text{adnexa, dermis})} = P_a / P_d$$

The total number of test points falling on profiles of the adnexa P_a and on the entire dermis P_d was counted. An estimator of the volume density of the adnexa was then calculated that is unbiased (that is, there is no systematic error due to the sampling or counting procedures) provided that the plane section and the test grid are randomly positioned.

Statistical analysis. To test for significant differences between percentage adnexa, the Student's two-tailed t-test function in Excel was used to calculate P values. Alpha was set at 0.05 and data are mean ± standard error.

Descriptive statistics. For strength measure, $n = 6$ for *M. musculus* and $n = 5$ for *A. kempi* and *A. percivali*. The following data are mean ± s.e.m. Mean failure strain (ε_f): *Mus* (0.61 ± 0.05), *A. kempi* (0.14 ± 0.05) and *A. percivali* (0.08 ± 0.02). Mean tensile strength (MPa): *Mus* (2.3 ± 0.19), *A. kempi* (0.15 ± 0.04), *A. percivali* (0.08 ± 0.03) and *Acomys* (both species) (0.11 ± 0.03). Mean toughness (MJ m^{-3}): *Mus* (0.77 ± 0.08), *A. kempi* (0.012 ± 0.006), *A. percivali* (0.005 ± 0.003) and *Acomys* (both species) (0.01 ± 0.004). The percentage of adnexa, $n = 6$ for each species. *A. percivali* ($55.61 \pm 4.28\%$) compared with *M. musculus* ($43.65 \pm 4.62\%$) ($t = 1.9$, $P = 0.043$). The percentage of wound contraction, $n = 12$ for *A. percivali* ($95.5 \pm 0.7\%$).

29. Gundersen, H. J. G. Notes on the estimation of the numerical density of arbitrary profiles: the edge effect. *J. Microsc.* **111,** 219–223 (1977).
30. Kiama, S. G., Maina, J. N., Bhattacharjee, J. & Weyrauch, K. D. Functional morphology of the pecten oculi in the nocturnal spotted eagle owl (*Bubo bubo africanus*), and the diurnal black kite (*Milvus migrans*) and domestic fowl (*Gallus gallus* var. *domesticus*): a comparative study. *J. Zool.* **254,** 521–528 (2001).
31. Weibel, E. R. *Stereological Methods* (Academic, 1979).